Three-dimensional spatio-temporal modelling of store operated Ca^{2+} entry: insights into ER refilling and the spatial signature of Ca^{2+} signals.

Emma McIvor, Stephen Coombes, Rüdiger Thul

Centre for Mathematical Medicine and Biology, School of Mathematical Sciences, University of Nottingham, University Park, Nottingham, NG7 2RD, UK

Abstract

The spatial organisation of Orai channels and SERCA pumps within ER-PM junctions is important for enhancing the versatility and specificity of sub-cellular Ca^{2+} signals generated during store operated Ca^{2+} entry (SOCE). In this paper we present a novel three dimensional spatio-temporal model describing Ca^{2+} dynamics in the ER-PM junction and sub-PM ER during SOCE. We investigate the role of Orai channel and SERCA pump location to provide insights into how these components shape the Ca^{2+} signals generated and affect ER refilling. We find that the organisation of Orai channels within the ER-PM junction controls the amplitude and shape of the Ca^{2+} profile but does not enhance ER refilling. The model shows that ER refilling is only weakly affected by the location of SERCA2b pumps within the ER-PM junction and that the placement of SERCA2a pumps within the ER-PM junction has much greater control over ER refilling.

Keywords:

Calcium signalling, ER-PM junctions, Mathematical modelling, Spatial Ca^{2+} signature, Orai channels, ER refilling

1. Introduction

Store operated Ca^{2+} entry (SOCE) is the influx of Ca^{2+} into the cytoplasm through Orai channels in the plasma membrane (PM) occurring in response to the depletion of Ca^{2+} from the endoplasmic reticulum (ER) [1, 2, 3, 4, 5]. This pathway for generating Ca^{2+} influx is important to the physiology of eukaryotic cells [6] as SOCE is involved in numerous cellular functions including endothelial cell proliferation [7], skeletal muscle contraction [8] and oocyte maturation [9]. Furthermore, abnormal SOCE has been linked to diseases, such as immunodeficiency [10] and inhibition of motor control in Purkinje neurons [11].

Stromal interaction molecule 1 (STIM1) resides in the ER membrane and acts as a Ca^{2+} sensor [12], initiating SOCE upon ER store depletion by directly coupling with and gating Orai channels, thus enabling Ca^{2+} influx into the cytoplasm [10, 13]. STIM1 interacts with a range of other channels and pumps and responds to additional cell stresses, such as hypoxic stress and changes in pH, and is considered to be a homeostatic regulator [3].

At rest, STIM1 and Orai diffuse along the ER membrane and PM [14], but upon store depletion STIM1 and Orai co-localise in distinct puncta or ER-PM junctions and bind together to form an active Orai channel [15, 16, 17, 18, 19, 20, 21]. ER-PM junctions occur in regions of the cell where the ER has extended towards the PM to ensure both membranes are closely apposed [21]. The distance between the PM and ER membrane has been estimated to be $10-20$nm [15, 16, 21] and this narrow gap between the membranes is key to SOCE activity and ER refilling [22, 23]. We will refer to this extension of

the ER as the 'sub-PM ER' and the non-junctional ER as the 'bulk ER'.

Experiments involving overexpression of STIM1 and Orai estimate that individual ER-PM junctions contain approximately 1,300 Orai channels [24], but the number of channels per junction expressed at physiological levels of STIM1 and Orai has not been recorded experimentally [25]. Analysis of electron micrographs [25] and comparisons of the total and single Orai channel currents [22] estimate there are $4-5$ endogenously expressed open Orai channels per ER-PM junction.

Upon Ca^{2+} influx, a microdomain of elevated Ca^{2+} is formed around an Orai channel and clustering of Orai channels causes the microdomains to overlap and create complex local Ca^{2+} signals [26, 22]. Sarco-endoplasmic reticulum Ca^{2+}-ATPase (SERCA) pumps transport Ca^{2+} from the ER-PM junction to the sub-PM ER, thus refilling the ER. SERCA pumps have been observed to co-localise with STIM1 in the ER-PM junction and are estimated to sit tens of nanometres away from the open Orai channels [27, 28, 29, 30, 31].

Ca^{2+} microdomains in the ER-PM junction are important for cell signalling as they provide specificity to local Ca^{2+} signals [23, 32, 33]. They allow direct activation of effectors residing within the microdomain and therefore enhance the ability to govern downstream cellular functions [26, 5, 25]. To fully appreciate the signalling potential of SOCE microdomains, it would be desirable to determine the range of Ca^{2+} concentrations in ER-PM junctions. However, this is difficult to measure experimentally because of the small dimensions of the ER-PM junctions [26], which are typically less than 300nm in diameter and $10-20$nm in height [22, 16, 15, 21].

Mathematical modelling allows us to make progress in this direction. Our

biologically constrained model can resolve Ca^{2+} signals occurring in small sub-cellular regions and thus supplement experimentally derived knowledge by acting as a lens to describe Ca^{2+} dynamics within ER-PM junctions. This will provide further information on Ca^{2+} dynamics and how a variety of cellular features, such as channel and pump placement, regulate the amplitude and spatial signature of local Ca^{2+} signals.

Mathematical models have previously been used to further our understanding of SOCE [34, 35, 25]. Using a modified whole cell Ca^{2+} model based on [36], Ong *et al.* [34] compared the level of SOCE activation induced by different decreases in the sub-PM ER and bulk ER Ca^{2+} concentrations. This model averages the Ca^{2+} concentrations within the ER-PM junction, sub-PM ER and bulk ER, so heterogeneous spatial Ca^{2+} profiles are not accounted for. In a similar vein, Croisier *et al.* [35] investigated averaged Ca^{2+} concentrations to shed light on how SOCE controls agonist induced Ca^{2+} oscillations in airway smooth muscle cells in the presence and absence of SERCA pump blockers. Samanta *et al.* [25] demonstrated that clustering of Orai channels stimulates gene expression and used mathematical modelling to examine the effect of clustering on spatial Ca^{2+} profiles. The three dimensional model showed that clustering elevates the amplitude of the Ca^{2+} signal and extends the radial spread of the microdomains. They proposed that such changes in the Ca^{2+} profile, as predicted by the model, could strengthen the signals activating gene expression.

In this paper we present a three dimensional spatio-temporal model to describe the Ca^{2+} dynamics occurring within the ER-PM junction and investigate the spatial signature of Ca^{2+} signals created during SOCE. We include

a sub-PM ER compartment to investigate the refilling properties of SOCE and allow Ca^{2+} transport between the domains through SERCA pumps on the ER membrane. The model is novel as it is the first to provide a spatio-temporal description of both the ER-PM junction and sub-PM ER domains and couple the spatially extended domains with SERCA pumps. We implement a mathematical framework with a high spatial resolution to enable simultaneous investigation of the refilling properties of SOCE and the key features controlling the spatial signature of Ca^{2+} signals.

In Section 2 we construct the mathematical model describing Ca^{2+} dynamics within both the ER-PM junction and sub-PM ER. We discuss the results predicted by the model in Section 3 and highlight the importance of Orai location on the shape of the Ca^{2+} profiles generated in the ER-PM junction. We investigate how Orai channel and SERCA pump location affects ER refilling and find that ER refilling is not enhanced by the clustered Orai channel configuration. Moreover, the placement of SERCA2a pumps has a greater impact on ER refilling than the placement of SERCA2b pumps in this situation. We discuss the implications of our results in more detail in Section 4.

This paper highlights the potential of mathematical modelling to examine the relationships between key components of SOCE, such as Orai channels and SERCA pumps, and thus further our understanding of how these components and their interactions regulate ER refilling and Ca^{2+} signalling. The paper also shows the ability of mathematical models to visualise highly spatially resolved Ca^{2+} profiles in sub-cellular domains, such as the ER-PM junction, which are too small for current Ca^{2+} imaging techniques.

2. Mathematical Model

We construct a three dimensional spatio-temporal mathematical model of SOCE which simulates ER refilling and describes the Ca^{2+} dynamics associated with this process. In this model we focus on capturing the fundamental properties of SOCE, ER refilling and the local Ca^{2+} signature, and include open Orai channels and SERCA pumps to facilitate these functions.

We illustrate the process we consider in Figure 1 where we have included open Orai channels in purple and SERCA pumps in green. SOCE is triggered by store depletion which results in movement of STIM1 towards the ER-PM junctions and ultimately co-localisation of active Orai channels and SERCA pumps within the ER-PM junctions. This is expected to occur on a time scale of approximately 40s [37]. Dynes *et al.* hypothesised that STIM1 binding to Orai holds the Orai channel in an open state and they did not observe stochastic single Orai channel opening while recording single channel dynamics [38]. Therefore, we assume that once the Orai channel is open it remains open until the ER is sufficiently refilled and STIM1 unbinds. We also neglect Ca^{2+} dependent inactivation at this time but this process will be included in future work. The open Orai channels allow a constant Ca^{2+} influx with an experimentally observed unitary current of 2.1fA [1, 39] and we assume the open channels are stationary during SOCE [38, 40, 4, 26, 14]. Figure 1(a) illustrates the arrangement of Orai channels and SERCA pumps in response to the depleted Ca^{2+} store of the sub-PM ER.

There are estimated to be 5 Orai channels per junction [25, 22] and the number of SERCA pumps present in the ER-PM junction is not known. We include ten SERCA pumps in our simulations for two reasons. Firstly, we

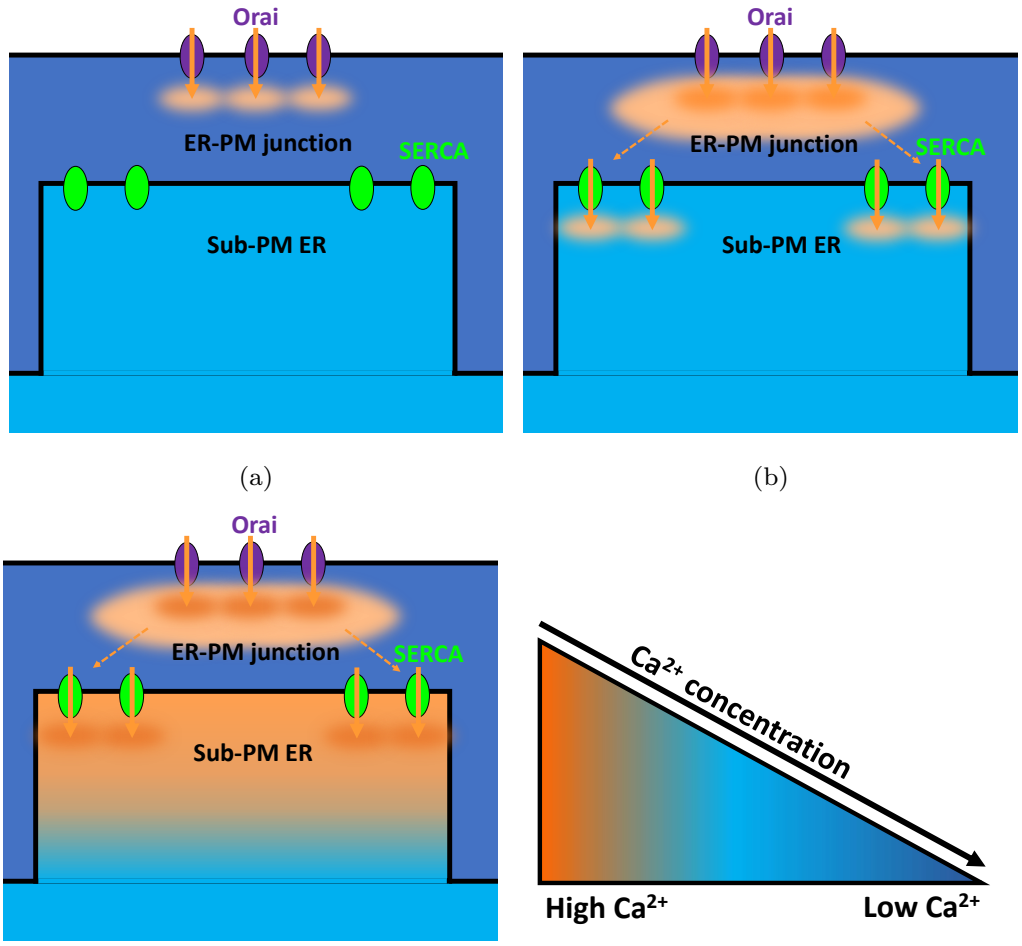

Figure 1: Illustration of the components of SOCE we include in our model and the relative Ca^{2+} concentrations. Not to scale. (a) Ca^{2+} influx through open Orai channels (purple). (b) Activation of SERCA pumps (green). (c) Refilling of sub-PM ER. (d) Colour scale showing relative Ca^{2+} concentrations.

did not want to overwhelm the Ca^{2+} dynamics occurring in the junction by including a large number of SERCA pumps. Secondly, the number of SERCA pumps present in a junction will be limited by the size of the ER-PM junction and the size of the individual pumps. Note that the number of SERCA pumps included can be adjusted in future work. We use the kinetic parameters as measured by Lytton *et al.* [41].

The Orai channel microdomains, seen by the orange puffs in Figure 1(a), occur as Ca^{2+} enters the ER-PM junction through the open Orai channels. These microdomains overlap and Ca^{2+} diffuses towards the ER membrane resulting in activation of SERCA pumps and initiating Ca^{2+} transport into the sub-PM ER, as shown in Figure 1(b). This leads to refilling of the Ca^{2+} stores of the bulk ER in Figure 1(c).

We assume that once Ca^{2+} enters the ER-PM junction or sub-PM ER Ca^{2+} movement within each domain is governed purely by diffusion, with membrane fluxes through either Orai channels or SERCA pumps transporting Ca^{2+} into or out of the domains. The high Ca^{2+} concentration around the channel mouth is thought to saturate local Ca^{2+} buffers [26, 33] so we follow the work of Samanta *et al.* [25] and Hogan [22] and use an unbuffered cytoplasmic diffusion coefficient, $D_{\mathrm{J}} = 220\mu\mathrm{m}^2\mathrm{s}^{-1}$, in the ER-PM junction [42]. The diffusion coefficient of Ca^{2+} in the ER lumen has not been definitively measured. However, crowding within the ER lumen is thought to slow Ca^{2+} diffusion [43, 44]. Dayel *et al.* [44] found diffusion within the ER lumen to be $3-6$ times slower than the bulk cytoplasmic diffusion coefficient and estimated the diffusion coefficient of Ca^{2+} in the ER lumen to be $5-10\mu\mathrm{m}^2\mathrm{s}^{-1}$. Swietach *et al.* measured the Ca^{2+} diffusion coefficient of the

SR lumen as $8 - 9\mu\text{m}^2\text{s}^{-1}$ [45] so in our model we use a diffusion coefficient, $D_{\text{ER}} = 10\mu\text{m}^2\text{s}^{-1}$, in the sub-PM ER. We assume the Ca^{2+} diffusion within the ER-PM junction and sub-PM ER is uniform in each direction.

2.1. Model geometry

The geometries of the the ER-PM junction and sub-PM ER are illustrated in Figure 2(a) with the Orai channels in purple and the SERCA pumps in green on the PM and ER membrane, respectively. We use estimates of the ER-PM junction dimensions [15, 16, 5, 25] to approximate the ER-PM junction by a cylinder of diameter 200nm and height 15nm where the upper face of the cylinder represents the PM and the lower face represents the ER membrane. The mantle of the cylinder represents the interface between the ER-PM junction and the rest of the cytoplasm. The sub-PM ER is closely apposed to the PM and extends out from the bulk ER so we approximate it by a cylinder of diameter 200nm. Here the upper face and mantle of the cylinder represent the ER membrane and the lower face represents the interface between the sub-PM ER and the bulk ER, which we refer to as 'Bulk_{int}'. The length of the sub-PM ER has not been experimentally recorded but we expect it to be considerably greater than the distance between the ER membrane and PM so we choose a cylinder of height of 485nm. This value can be easily altered in future work when more information about the dimensions of the sub-PM ER is available.

2.1.1. Boundary conditions

The ER-PM junction is contained within the PM and ER membrane and the sub-PM ER is bounded by the ER membrane. In our model, Ca^{2+}

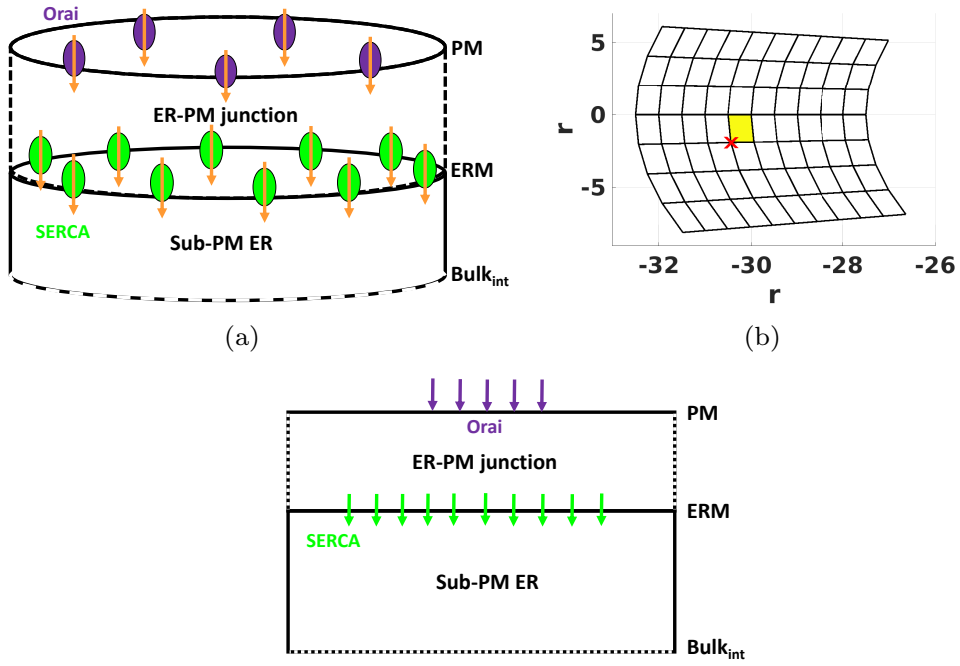

Figure 2: (a) Illustration of the model geometry of the ER-PM junction and sub-PM ER with Orai channels (purple) and SERCA pumps (green) placed on the PM and ER membrane (ERM), respectively. (b) Discretisation of the grid along a horizontal cut. The shaded yellow grid element approximates Ca^{2+} influx through a single channel and the red cross represents the coordinates to identify the grid element. (c) Diagram showing the boundary conditions imposed on the domains. Orai channel and SERCA pump fluxes are represented by purple and green arrows, respectively. Solid black lines in (a) and (c) represent membranes with flux boundary conditions and dashed black lines represent the interface between the ER-PM junction and bulk cytoplasm and the interface between the sub-PM ER and bulk ER (Bulk_{int}), respectively.

crosses these boundaries only by passing through Ca^{2+} channels or pumps. We discretise each domain according to the parameters in Table A.2. We approximate Ca^{2+} flux through a single channel by Ca^{2+} flux through one grid element, shaded yellow in Figure 2(b). Each grid element can be uniquely referenced by the location of one of its corners. For example, the yellow grid element in Figure 2(b) can be identified with the coordinates $(\overline{r}, \overline{\phi})$, which are shown as a red cross.

Fluxes through Orai channels are represented by purple arrows and fluxes through SERCA pumps are represented by green arrows in Figure 2(b). The remaining parts of the membranes are impenetrable, which we capture by imposing 'no flux' boundaries to prevent Ca^{2+} from diffusing freely across the boundary. These 'no flux' boundaries are represented by the solid black lines in Figure 2(c).

Ca^{2+} microdomains greatly increase the Ca^{2+} concentration in the immediate vicinity of the channel or pump but this elevation declines steeply as the distance from the channel increases [26, 46]. We do not expect a noticeable increase in Ca^{2+} concentration at the interface between the ER-PM junction and bulk cytoplasm because of the sharp decline in Ca^{2+} elevation at the edge of the ER-PM junction. Therefore, the Ca^{2+} concentration at the interface between the ER-PM junction and bulk cytoplasm is chosen to be the same as the Ca^{2+} concentration of the bulk cytoplasm, 0.1μM. Similarly, we expect the Ca^{2+} concentration at the interface between the sub-PM ER and bulk ER to be equal to the Ca^{2+} concentration of the depleted bulk ER as at such distances from the SERCA pumps we expect little increase in the Ca^{2+} concentration during the simulations. We have chosen the Ca^{2+}

concentration at the interface between the sub-PM ER and bulk ER to be 150μM. These 'fixed value' boundary conditions are shown as dashed lines in Figure 2(c).

2.2. Modelling Ca^{2+} *dynamics*

We define C_J and C_S to be the Ca^{2+} concentrations in the ER-PM junction and the sub-PM ER, respectively. We simulate the Ca^{2+} dynamics in each domain using the diffusion equations,

$$\frac{\partial C_J}{\partial t} = D_J \nabla^2 C_J, \tag{1}$$

and

$$\frac{\partial C_S}{\partial t} = D_{ER} \nabla^2 C_S, \tag{2}$$

and the boundary conditions as shown diagrammatically in Figure 2(c). The model describes the system after the ER Ca^{2+} stores have been depleted and as Ca^{2+} influx via Orai channels is about to occur. Initially there is no Ca^{2+} influx into the ER-PM junction so our initial Ca^{2+} concentration is the baseline cytosolic Ca^{2+} concentration, $[Ca^{2+}]_i = 0.1\mu$M. We have depleted the Ca^{2+} store in the sub-PM ER from a resting concentration of $[Ca^{2+}]_{ER} \approx 400\mu$M [4] to 150μM to take account of the greater depletion observed in the sub-PM ER by Ong *et al.* [34] and to ensure significant I_{CRAC} activation, for which a dissociation constant of $K_{1/2} = 169\mu$M has been reported [47].

We solve the spatial aspect of the diffusion equation using Green's functions and the method discussed in Appendix A to derive the exact solution of this system. Alternative approaches involving purely numerical techniques,

such as finite element methods, are also applicable; however, we do not pursue those approaches. We use the exact solution to pre-compute key components of our solution therefore reducing the computational cost of each time step during the simulation. We iterate the spatial solution over each time step to simulate the temporal evolution of the Ca^{2+} profiles. Using this approach we can simulate the spatial Ca^{2+} concentrations in the ER-PM junction and sub-PM ER at each time step and then evolve the Ca^{2+} concentrations over time to simulate the spatio-temporal Ca^{2+} dynamics of the whole system. The code for this model is available online and details of the code and the processing times for the simulations in this study are provided in Appendix A.

3. Results

3.1. Clustering of Orai channels creates spatially distinct Ca^{2+} *profiles in the ER-PM junction*

We compare the Ca^{2+} profiles generated by Orai channels in a clustered and non-clustered configuration to examine the effect of clustering on the spatial signature of the Ca^{2+} signals. Samanta *et al.* [25] estimated the inter-channel distance of an Orai channel and its nearest neighbour to be 47nm. We place the Orai channels in a ring with an inter-channel distance of 39nm when the channels are clustered, so the channels are placed closer together than the nearest neighbour estimate. When the channels are non-clustered we use an inter-channel distance of 65nm, so the channels are more widely spaced than the nearest neighbour estimate. Manjarres *et al.* observed SERCA2b pumps co-localising to the ER-PM junction and proposed that

SERCA2b pumps form a ring like structure surrounding the Orai channels in the ER-PM junction [27, 28, 29, 31]. We place the Orai channels and SERCA pumps in concentric rings, as depicted in Figures 3(a) and 3(b).

The Ca^{2+} profiles at the PM generated by the clustered and non-clustered Orai distributions are shown in Figures 3(c) and 3(d). The magnitude of the Ca^{2+} concentrations are similar, approximately 60μM, but we observe different patterns for each Orai distribution. The Orai channel microdomains overlap more when the channels are clustered which results in a larger region of elevated Ca^{2+}, reaching Ca^{2+} concentrations of around 7μM in the centre of the ER-PM junction. The microdomains of the non-clustered channels overlap to a lesser extent with Ca^{2+} concentrations of approximately 4μM.

The differences in the spatial Ca^{2+} concentrations generated by clustered and non-clustered Orai channels are even more prominent at the ER membrane, as seen in Figures 3(e) and 3(f). The microdomains of the clustered Orai channels merge into one region of elevated Ca^{2+} and the individual channel microdomains are completely absorbed into this Ca^{2+} pattern. However, the microdomains of the non-clustered channels are still distinguishable as circles inside the star shaped region of elevated Ca^{2+} in Figure 3(f). The clustered configuration attains Ca^{2+} concentrations of around 7μM along the ER membrane whereas the Ca^{2+} concentrations generated by the non-clustered channels peak at approximately 4.5μM.

We directly compare the Ca^{2+} profiles generated at Orai channels on the PM in Figure 4(a) by plotting the Ca^{2+} profiles at a location represented by the dashed black lines in Figures 3(c) and 3(d). At the PM, we see that the clustered channel configuration (blue line) results in greater elevation of Ca^{2+}

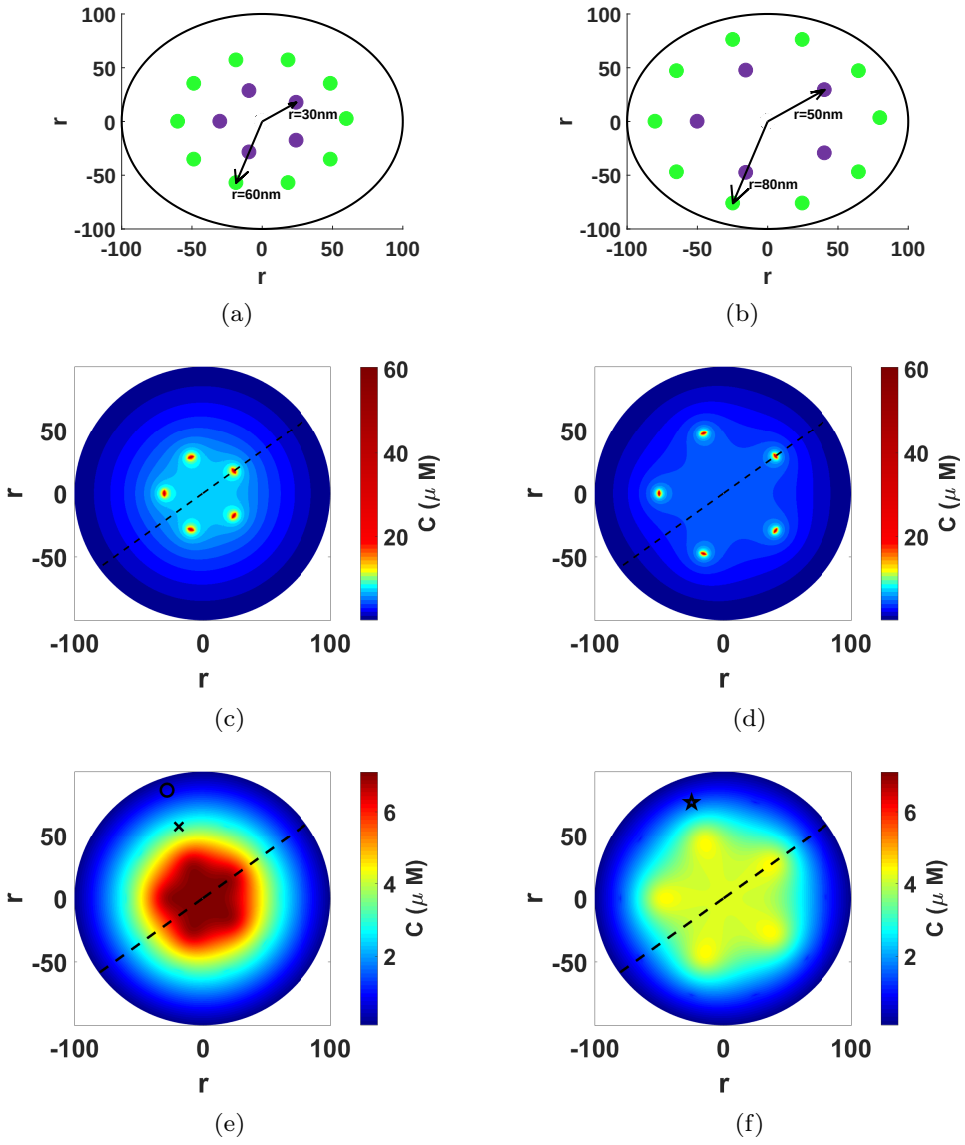

Figure 3: (a,b) Illustrations of the placement of Orai channels (purple) on the PM in a clustered and non-clustered configuration with SERCA pumps (green) placed 30nm away. (c,d) Ca^{2+} profiles at the PM when Orai channels are clustered and non-clustered. (e,f) Ca^{2+} profiles at the ER membrane when Orai channels are clustered and non-clustered. Parameters as in Tables A.1 and A.2 and non-clustered mesh has parameters $\triangle\phi = 0.0251$ and $\sigma_\phi = 0.03$ to ensure the size of the Orai channel is the same in both the clustered and non-clustered Orai channel configurations.

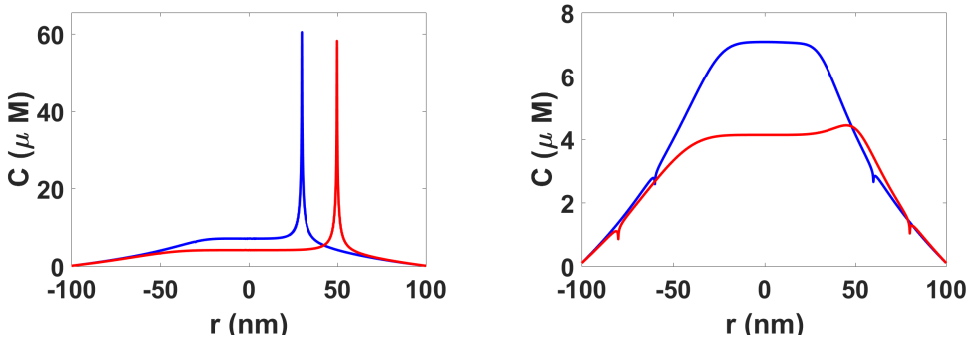

(a) (b)

Figure 4: (a) Ca^{2+} profiles at the PM along the black dashed lines in Figures 3(c) and 3(d). (b) Ca^{2+} profiles at the ER membrane along the black dashed lines in Figures 3(e) and 3(f). The blue and red lines represent the Ca^{2+} profiles arising from the clustered and non-clustered Orai channel distributions, respectively. Parameters as in Tables A.1 and A.2.

concentrations around $r = 0$ than the non-clustered channels (red line). This increased amplitude occurs because the clustered microdomains overlap to a greater extent than the non-clustered microdomains. By comparing the Ca^{2+} profiles at the ER membrane directly beneath the Orai channels in Figure 4(b), we see that clustering of Orai channels (blue line) greatly increases the magnitude of the Ca^{2+} concentrations achieved in the ER-PM junction. The clustered configuration reaches Ca^{2+} concentrations of 7μM which is almost 50% greater than the Ca^{2+} concentrations of 4.4μM generated by the non-clustered configuration. We observe small dips in the Ca^{2+} profiles at the ER membrane in Figure 4(b) corresponding to Ca^{2+} efflux from the ER-PM junction via SERCA pumps. The difference in the Ca^{2+} concentrations demonstrates that clustering of Orai channels controls the amplitude of the Ca^{2+} profile and creates spatially distinct Ca^{2+} profiles. Samanta *et al.*

observed that confinement of Orai channels within the ER-PM junctions led to increased c-fos and NFAT activation [25]. Using a three-dimensional model of an ER-PM junction, they found that clustering of Orai channels increased the Ca^{2+} concentrations on the ER surface and proposed that the ability to control the local spatial Ca^{2+} signal via clustering would result in more effective activation of c-fos gene expression and NFAT. Our model demonstrates that the inter-channel distance is an important parameter for governing the amplitude and shape of Ca^{2+} signals generated in the ER-PM junction. Therefore, the ability of Orai channels to cluster provides a mechanism by which Ca^{2+} can specifically activate distinct downstream signalling processes, such as NFAT [48], by controlling the amplitude and shape of the Ca^{2+} signal.

3.2. Clustering Orai channels does not enhance ER refilling

ER refilling requires SERCA pumps to transport Ca^{2+} from the ER-PM junction to the sub-PM ER and the level of SERCA pump activity depends on the Ca^{2+} concentration surrounding the pumps. We measure the activity of the SERCA pumps in terms of the maximal activity possible, where 100% corresponds to a maximally activated SERCA pump. We have seen in Section 3.1 that clustering increases the local Ca^{2+} concentrations in the ER-PM junction, so in this section we investigate whether clustering results in more highly activated SERCA2b pumps leading to increased rates of ER refilling. We fix the distance between the Orai channels and SERCA2b pumps to ensure that any change in ER refilling is solely attributed to the Orai channel arrangement.

In our simulations we find that the Ca^{2+} profile within the ER-PM junc-

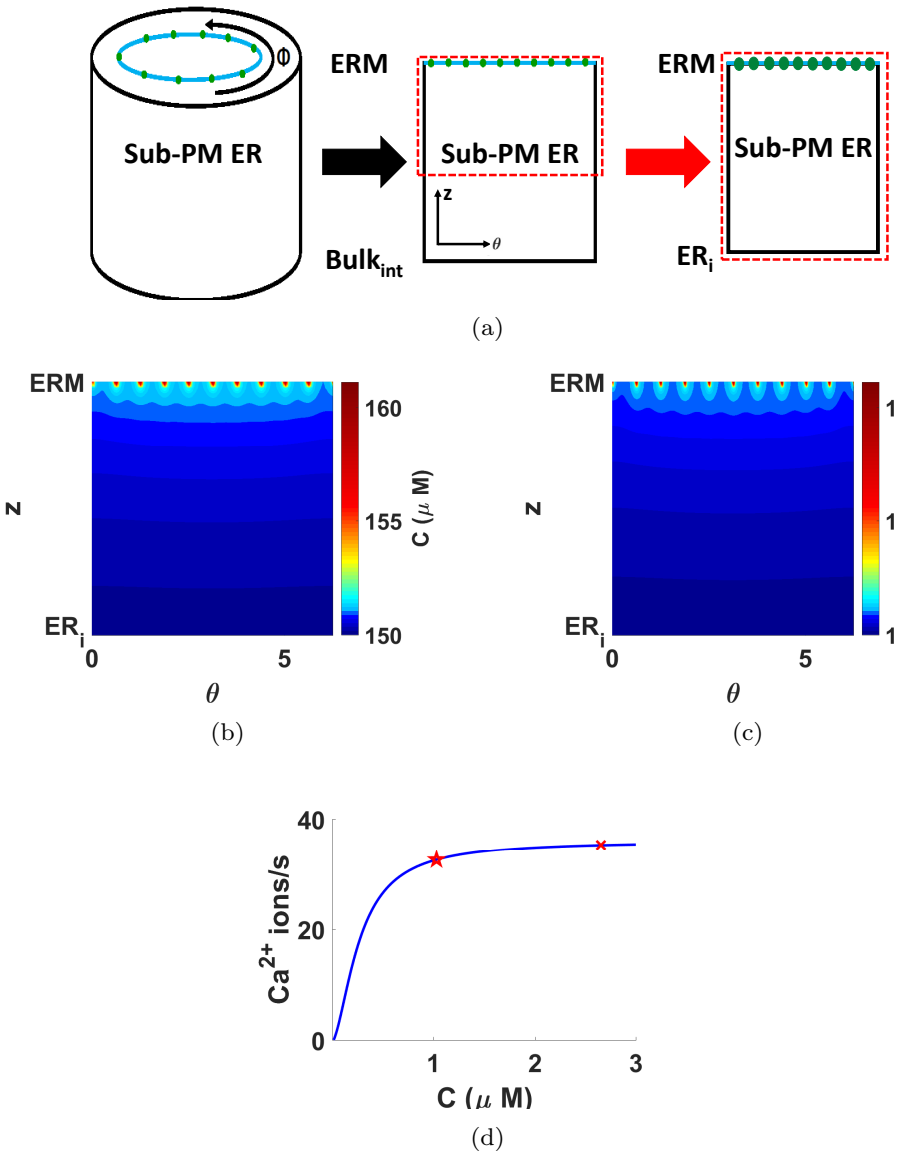

Figure 5: (a) Diagram explaining how we visualise the Ca^{2+} concentration in the sub-PM ER. The green circles represent the SERCA pumps on the ER membrane. (b,c) Ca^{2+} profiles generated in the sub-PM ER along the ring of SERCA2b pumps in response to a clustered and non-clustered Orai channel distribution. (e) Plot of the Ca^{2+} transport activity of SERCA2b. The red cross and star correspond to the transport activity in response to the clustered and non-clustered Orai channels, respectively. Parameters as in Tables A.1 and A.2 and non-clustered mesh has parameters $\triangle\phi = 0.0251$ and $\sigma_\phi = 0.03$.

tion reaches an equilibrium concentration profile in less than 0.25ms. The resulting SERCA2b pump fluxes, and therefore activity, will remain constant once this equilibrium state has been achieved. Therefore, SERCA2b pump activity after 1ms will be the same as the SERCA2b pump activity after a longer time, provided the Orai channel has not switched off and disturbed the equilibrium fluxes. It is important to note that the time to achieve an equilibrium Ca^{2+} profile within the ER-PM junction depends on the Ca^{2+} channels and pumps included in the junction. Additional interactions, such as PMCA activity, could prevent or delay attainment of an equilibrium Ca^{2+} profile in which case the early ER refilling will not be representative of the long term ER refilling. In our simulations we find that the Ca^{2+} profile in the ER-PM junction reaches an equilibrium concentration within 0.25ms so the early refilling will be representative of the long term ER refilling in this study.

SERCA2b pumps are the only component in the model that transports Ca^{2+} into the sub-PM ER to refill the depleted Ca^{2+} store. Therefore, the rate of ER refilling depends on the SERCA2b pump activity and greater SERCA2b pump activity results in faster ER refilling. We can consider the SERCA2b pump activity in response to clustered and non-clustered Orai to compare the rate of ER refilling achieved in response to each Orai channel distribution. As the SERCA2b pump activity remains constant, the level of ER refilling will proceed at the same rate while the ER-PM junction is in equilibrium. This means that although the ER will have been refilled to a greater extent after a longer amount of time the rate of ER refilling with the clustered and non-clustered Orai channels will be the same at both early

and late times. As we are concerned with the rate of ER refilling for the clustered and non-clustered Orai channels, and not the total magnitude of ER refilling, we will compare the Ca^{2+} profiles after 1ms.

The SERCA2b pumps denoted by the black cross and star in Figures 3(e) and 3(f) are placed a distance of 30nm from the clustered and non-clustered Orai channels, respectively. The Ca^{2+} concentration surrounding the SERCA2b pumps is higher in the clustered Orai configuration than the non-clustered configuration. The different Ca^{2+} concentrations around the SERCA2b pumps are seen in Figure 4(b). The SERCA2b pumps are situated at the dips in the Ca^{2+} profile at concentrations of approximately 2.658μM and 1.032μM in the clustered and non-clustered Orai configurations, respectively. The SERCA2b pumps are highly activated in both Orai distributions, but there is a slight decrease in SERCA2b activity from 98% with the clustered Orai channel distribution to 90% when the channels are non-clustered. Therefore, the rate of ER refilling is very similar for both the clustered and non-clustered Orai channel distributions.

We are interested in the rate of ER refilling but we can show the extent of Ca^{2+} refilling in the sub-PM ER after 1ms to allow a visual and more intuitive comparison of the ER refilling occurring in response to the clustered and non-clustered Orai channels. We take a slice along the blue line in Figure 5(a) on which the SERCA2b pumps sit and 'unfurl' this slice to visualise the Ca^{2+} concentration throughout the sub-PM ER beneath the SERCA2b pumps. We then focus on the section of the sub-PM ER from an internal point of the sub-PM ER (ER_i) to the ER membrane, enclosed by the red dashed rectangle in Figure 5(a). Focusing on this section of the sub-PM ER allows

us to capture the structure of the Ca^{2+} patterns produced during refilling of the ER via SERCA pumps. We can then consider the extent to which Ca^{2+} diffuses from the ER membrane to compare the relative levels of ER refilling.

We show the extent to which Ca^{2+} has diffused from the SERCA2b pumps when the Orai channels are clustered and non-clustered in Figures 5(b) and 5(c). As the SERCA2b pumps transport Ca^{2+} into the sub-PM ER regions of elevated Ca^{2+} are created around the SERCA2b pumps. These regions overlap when the Orai channels are clustered as the SERCA2b pumps are closer together, so SERCA2b pump placement also creates local Ca^{2+} patterns in the sub-PM ER. We observe that the maximum Ca^{2+} concentrations achieved after 1ms are approximately 160μM which is an increase of 10μM. Jousset *et al.* found that the ER Ca^{2+} store is refilled within two minutes [49]. Therefore, we would not expect to see significant levels of refilling after 1ms. However, the extent of Ca^{2+} diffusion after 1ms within the sub-PM ER is very similar for the clustered and non-clustered Orai distributions. This further demonstrates that the rate of ER refilling is roughly equal in both cases.

In Figure 5(d) we compare the Ca^{2+} transport rates of SERCA2b in response to clustered and non-clustered Orai channel distributions. The activity of the SERCA2b pumps are shown by the red cross and red star, respectively. As we can see, the decrease in Ca^{2+} concentration surrounding the SERCA2b pumps when Orai channels are clustered and non-clustered, predicted from the simulations, does not result in a great decrease in the SERCA2b Ca^{2+} transport rate. So, although clustering increases Ca^{2+} concentrations in the ER-PM junction, ER refilling is not enhanced by Orai

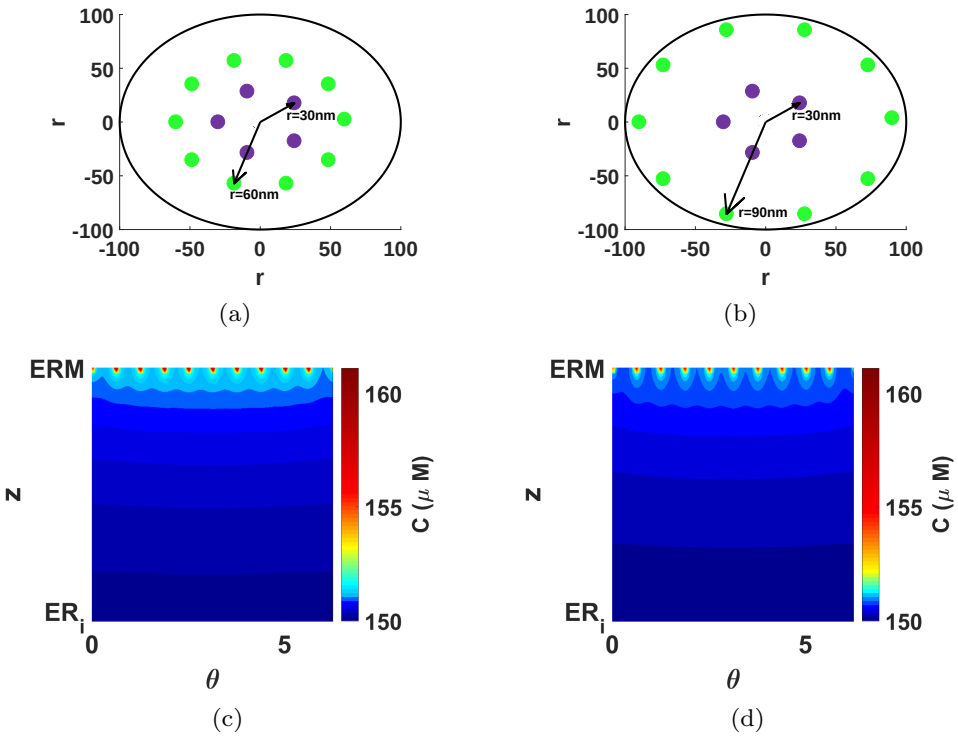

Figure 6: (a,b) Illustrations of the placement of Orai channels (purple) on the PM in a clustered configuration with SERCA pumps (green) placed 30nm or 60nm away. (c,d) Ca^{2+} profiles generated in the sub-PM ER along the ring of SERCA2b pumps 30nm and 60nm from the Orai channels. Parameters as in Tables A.1 and A.2.

channel clustering.

3.3. The distance between Orai channels and SERCA2b pumps is not a major regulator of ER refilling

In the previous section, we demonstrated that clustering does not enhance ER refilling, so we now focus on the second factor which could control SERCA pump activity and ER refilling: the distance between Orai channels and SERCA pumps.

The peripheral Ca^{2+} concentration is roughly equal for clustered and non-clustered Orai channel distributions (see Figure 4). We therefore consider clustered Orai channels only, to ensure that any results are a consequence of the distance between channels and pumps. We place the SERCA2b pumps at distances of 30nm and 60nm from the Orai channels, as illustrated in Figures 6(a) and 6(b). This approach can determine how the proximity of SERCA2b pumps to Orai channels affects the rate of ER refilling. As in Section 3.2, we are concerned with the rate of ER refilling and not the total magnitude of ER refilling. In this section we compare ER refilling after 1ms when the SERCA2b pumps are placed 30nm and 60nm from the Orai channels to investigate how the placement of the SERCA2b pumps affects the rate of ER refilling.

The black cross and circle in Figure 3(e) represent the SERCA2b pumps at distances of 30nm and 60nm from the Orai channels. Ca^{2+} microdomains are characterised by a steep decrease in Ca^{2+} concentration away from the Orai channels, which can be seen in Figure 3(e). This ensures that the SERCA2b pumps are exposed to different Ca^{2+} concentrations when placed close to and far from the Orai channels. Such decreases in the Ca^{2+} concentrations surrounding the SERCA2b pumps could reduce the activity of the SERCA2b pump and potentially reduce the rate of ER refilling.

The simulated SERCA2b pump activity 30nm and 60nm from the Orai channels is 98% and 73%, respectively. The pumps are highly activated close to the Orai channels, but continue working well above half maximal activity even in peripheral locations. This suggests that even though there is a decrease in SERCA2b activity, ER refilling will still proceed at a sufficiently

high rate to ensure the ER is refilled, although it will be slightly slower.

After 1ms, we compare the Ca^{2+} concentrations in the sub-PM ER directly beneath the SERCA2b pumps in Figures 6(c) and 6(d). The Ca^{2+} concentration profiles are similar and the sub-PM ER is refilled to the same extent by SERCA2b pumps placed at both locations within the ER-PM junction. Ca^{2+} from the SERCA2b pumps has diffused similar distances away from the ER membrane with each SERCA2b pump placement.

This suggests that ER refilling does not depend greatly on the placement of SERCA2b pumps. The pumps located further from the Orai channel will refill the ER at a slower rate but the increased distance does not drastically reduce the rate of ER refilling. Therefore, the proximity of SERCA2b pumps to Orai channels is not a major regulator of ER refilling.

3.4. The placement of SERCA2a pumps has a greater impact on ER refilling than the placement of SERCA2b pumps

In Section 3.3 we examined how the proximity of SERCA2b pumps to Orai channels impacted ER refilling and demonstrated that the placement of SERCA2b pumps within the ER-PM junction only weakly affected ER refilling. Sampieri *et al.* observed SERCA2a pumps co-localising to the ER-PM junction during SOCE [30]. SERCA2a and SERCA2b are functionally distinct with SERCA2a having a lower affinity for Ca^{2+} and higher Ca^{2+} turnover rate [50, 41]. Such different kinetic parameters could result in different ER refilling dynamics depending on the type of SERCA pump isoform. In this section we include only SERCA2a pumps to investigate how the placement of SERCA2a pumps affects the rate of ER refilling. We again find that the ER-PM junction reaches an equilibrium Ca^{2+} concentration profile within

less than 0.25ms and the SERCA2a fluxes are constant after this equilibrium is reached. Therefore, we compare the rates of ER refilling after 1ms as they will be representative of the long term ER refilling rate.

As in the previous section, we consider only the clustered Orai channel arrangement and only include SERCA2a pumps to ensure that our results are a direct consequence of the distance between Orai channels and SERCA2a pumps. We illustrate the placement of the Orai channels and SERCA pumps in Figures 6(a) and 6(b), where the green circles now represent SERCA2a pumps at distances of 30nm and 60nm from the Orai channels, respectively.

The Ca^{2+} microdomains generated around the Orai channels ensure that the Ca^{2+} concentrations surrounding the SERCA2a pumps placed 30nm are larger than the concentrations surrounding the SERCA2a pumps 60nm from the Orai channel (see Figure 3(e)). Again, this reduction in Ca^{2+} concentration could control the level of SERCA2a activity and thus regulate ER refilling.

The simulated SERCA2a pump activity 30nm and 60nm from the Orai channels is 98% and 52%, respectively. As with the SERCA2b pumps, we see that the SERCA2a pumps located 30nm from the Orai channels are very highly activated. However, the SERCA2a pumps located peripherally within the ER-PM junction are working only slightly above half maximal activity. Therefore, the distance between SERCA2a pumps and Orai channels is an important factor controlling SERCA2a activity as increasing the distance between the Orai channel and SERCA2a pump halves SERCA2a pump activity thus drastically reducing the ER refilling rate.

We compare the Ca^{2+} concentrations in the sub-PM ER directly beneath

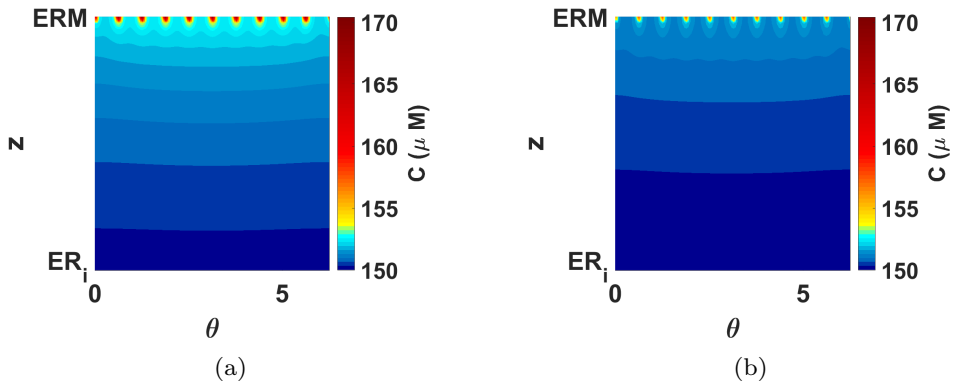

Figure 7: (a,b) Ca^{2+} profiles generated in the sub-PM ER along the ring of SERCA2a pumps 30nm and 60nm from the Orai channels. Parameters as in Tables A.1 and A.2.

the SERCA2a pumps in Figures 7(a) and 7(b). After 1ms, Ca^{2+} from the SERCA2a pumps placed 30nm from the Orai channels has diffused much further than Ca^{2+} from SERCA2a pumps placed 60nm from the Orai channels. Therefore, placing SERCA2a pumps 30nm from the Orai channels results in faster ER refilling than SERCA2a pumps placed 60nm from the Orai channels. In fact, the SERCA2a pumps 30nm from the Orai channels achieve Ca^{2+} concentrations of 170μM within 1ms whereas the SERCA2a pumps 60nm from the Orai channels only attain Ca^{2+} concentrations of approximately 160μM. Given that the depleted ER concentration is 150μM, this shows that ER refilling is twice as fast when SERCA2a pumps are closer to the Orai channels, which is what we expect since the pumps 60nm from the channels are working at approximately 50% activity levels.

This difference in the rates of ER refilling suggests that the placement of SERCA2a pumps in the ER-PM junction and in particular their proximity to Orai channels controls the rate of ER refilling.

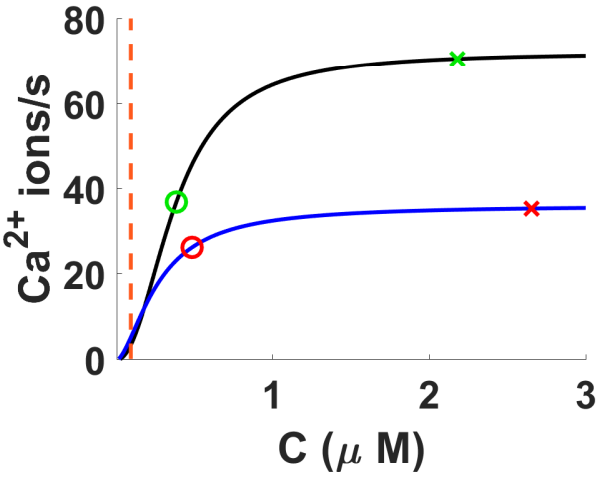

(a)

Figure 8: Ca^{2+} transport rates of SERCA2a and SERCA2b pumps represented by the black and blue curves, respectively. Green circle and triangle denote clustered Orai channel arrangements with SERCA2a pumps placed 30nm and 60nm away, respectively. Red circle and triangle denote clustered Orai channel arrangements with SERCA2b pumps placed 30nm and 60nm away, respectively. The dashed orange line represents the baseline Ca^{2+} concentration of the ER-PM junction, $[Ca^{2+}]_i = 0.1\mu$M.

SERCA pumps are the only structures in our model capable of transporting Ca^{2+} from the ER-PM junction into the sub-PM ER so the SERCA pump Ca^{2+} transport activity is a measure of the ER refilling rate, with higher SERCA pump Ca^{2+} transport activity corresponding to faster ER refilling. We compare the SERCA pump Ca^{2+} transport activity for both SERCA2a and SERCA2b pumps in Figure 8. We plot the Ca^{2+} transport rate against Ca^{2+} concentration and the black and blue curves represent the SERCA2a and SERCA2b Ca^{2+} transport rates, respectively. The green (red) crosses and circles represent the activity levels of SERCA2a (SERCA2b) pumps placed 30nm and 60nm from the clustered Orai channels. The dashed orange line represents the baseline Ca^{2+} concentration of the ER-PM junction, $[Ca^{2+}]_i = 0.1\mu$M. In Figure 8 we see that both SERCA pumps have similar Ca^{2+} transport rates at Ca^{2+} concentrations just above the resting Ca^{2+} concentration and that the distance between Orai channels and SERCA pumps has a much greater impact on the Ca^{2+} transport rate of SERCA2a than SERCA2b.

Although we can plot the SERCA Ca^{2+} transport curves in Figure 8 we cannot predict the activity of the SERCA pumps without knowing the Ca^{2+} concentrations in the ER-PM junction. This information is not available before we simulate SOCE as we cannot measure the Ca^{2+} concentrations experimentally. Therefore, it is necessary to simulate SOCE to be able to predict the local Ca^{2+} concentrations and SERCA activities and thus compare the rates of ER refilling. The simulations of the Ca^{2+} concentrations within the sub-PM ER provide a second method of measuring and comparing the ER refilling occurring as we visualise the Ca^{2+} profiles within the

sub-PM ER.

Therefore, although the arrangement of Orai channels and placement of SERCA2b pumps have minor influences on ER refilling the key factor controlling ER refilling is the placement of SERCA2a pumps and in particular, their proximity to Orai channels.

4. Discussion and Conclusion

We have constructed a three dimensional spatio-temporal model to simulate the Ca^{2+} dynamics in the ER-PM junction and sub-PM ER. Our model provides a means to visualise Ca^{2+} profiles in signalling microdomains on a nanometre scale, thus offering a highly spatially resolved view on local Ca^{2+} behaviour. Using this high spatial resolution we were able to investigate the impact of placement of signalling components, such as Orai channels and SERCA pumps, on the Ca^{2+} signals generated in response to SOCE and their effect on ER refilling.

The model shows that clustering of Orai channels causes Ca^{2+} microdomains to overlap leading to higher local Ca^{2+} concentrations in the ER-PM junction. The Ca^{2+} profiles generated by clustered and non-clustered profiles had distinct shapes and also attained different peak Ca^{2+} concentrations. The magnitude and shape of Ca^{2+} signals in the ER-PM junction could control activation of a range of downstream cellular functions [48], such as NFAT activation as hypothesised by Samanta *et al.* [25]. Therefore, clustering could act as a mechanism to create structured Ca^{2+} profiles ensuring sufficiently high Ca^{2+} concentrations are attained in regions of the signalling junction to activate specific effector molecules. The highly heterogeneous Ca^{2+} pro-

files also have the potential to activate a diverse range of effector molecules within the junction in a controlled manner by targeting the molecules to regions of the junction according to the specific Ca^{2+} binding coefficients of each molecule [25, 26, 22, 51].

In this paper we considered the importance of the locations of Orai channels and SERCA pumps within the ER-PM junction. We investigated the relationship between ER refilling and the inter Orai channel distance as well as the relationship between ER refilling and Orai-SERCA distance. Our results show that the rate of ER refilling is not greatly impacted by clustering of Orai channels or the placement of SERCA2b pumps. However, the rate of ER refilling does depend on the distance between SERCA2a pumps and Orai channels.

When SERCA2b pumps are placed 30nm away from the Orai channels, SERCA2b pump activity in both the clustered and non-clustered Orai channel configuration is high ($\geq 90\%$). Although the Ca^{2+} concentration increases with clustered Orai channels, this does not correspond to a considerable increase in the Ca^{2+} transport rate of the SERCA2b pump, as seen in Figure 5(d). The reason for this is that SERCA pump activity only increases in small increments as it approaches its maximal activity level. Therefore, the rate of ER refilling is not enhanced by clustering Orai channels. Moving towards the periphery of the ER-PM junction, we observed a decrease in the Ca^{2+} concentration. Concomitantly, SERCA2b and SERCA2a pump activity was reduced from 98% to 72% and 98% to 52%, respectively, when the distance between Orai channels and SERCA pumps was increased from 30nm to 60nm. The rate of ER refilling was similar for both distances with

SERCA2b pumps but greatly reduced with SERCA2a pumps. We compared the Ca^{2+} transport rates of both SERCA2a and SERCA2b in Figure 8 and found SERCA2a to be much more sensitive to the observed Ca^{2+} concentration than SERCA2b, thus leading to greater control over ER refilling.

This initial model focuses on the fundamental properties of SOCE: ER refilling and the associated Ca^{2+} patterns. Through further development and refinement of the model, we will include more components of Ca^{2+} signalling, such as PMCA pumps, and regulatory mechanisms, such as Ca^{2+} dependent inactivation of the Orai channel, to provide a more physiologically realistic description of SOCE. Currently, the model is not cell type specific, but including cell specific parameters, such as binding coefficients, and cell specific structures in the future will allow the model to be tailored for specific cell types.

In conclusion, our model uncovers a novel way to simulate and visualise the highly heterogeneous Ca^{2+} concentrations generated in small sub-cellular compartments during SOCE. Using simulations of specific Orai channel and SERCA pump distributions affords a way to predict the spatial signature of the Ca^{2+} signals in the ER-PM junction and sub-PM ER. This can be used to further investigate how interactions between Orai channels and SERCA pumps generate distinct Ca^{2+} signals, which could regulate downstream cellular signals. For the first time, the model includes a spatially extended sub-PM ER domain to enable investigation into mechanisms governing ER refilling to provide further insight into the importance of specific components of SOCE. The model demonstrates that the amplitude and shape of Ca^{2+} signals throughout the ER-PM junction are strongly controlled by the Orai

channel distribution. We also find that clustering of Orai channels and placement of SERCA2b pumps within the ER-PM junction have very little impact on the rate of ER refilling. However, the distance between SERCA2a pumps and Orai channels is a major factor for determining ER refilling.

Further work is required to fully address the relationship between the microscale patterning of the Ca^{2+} signal within the ER-PM junction and whole cell responses such as gene expression. Currently, Ca^{2+} imaging techniques cannot resolve the local Ca^{2+} signals, however, mathematical modelling can predict the shape of the Ca^{2+} signals generated in response to a variety of Orai channel distributions and compare the Ca^{2+} concentrations achieved. The levels of gene expression, observed in response to different Orai channel distributions, can be directly measured using experimental techniques. Mathematical modelling can provide insight to the microscale patterning of Ca^{2+} profiles created within ER-PM junctions and by combining this insight with whole cell observations we can develop a deeper understanding of how Orai channel clustering regulates whole cell behaviour such as NFAT expression.

Appendix A. Mathematical model

In Section 2.2 we described the spatio-temporal model diagrammatically; here, we discuss the mathematical model in greater depth. The simulations throughout the paper use the parameter values in Tables A.1 and A.2 unless otherwise specified.

Mathematical modelling has previously been employed to enhance understanding of SOCE [34, 25]. The model presented by Ong *et al.* [34] examines

Parameter	Description	Value	Unit
D_J	Diffusion coefficient in ER-PM junction	220 [22, 42]	$\mu m^2 s^{-1}$
D_{ER}	Diffusion coefficient in ER-PM junction	10 [45, 44]	$\mu m^2 s^{-1}$
a	Radius of junction	100 [25, 26]	nm
H	Distance to PM	2500	nm
L_2	Distance to ER membrane	2485	nm
L_1	Distance to interface between sub-PM ER and bulk ER	2000	nm
ER_i	Distance to internal point of sub-PM ER (see Figure 5(a))	2286.15	nm
I_{Orai}	Orai single channel current	2.1 [1, 39]	fA
F	Faraday's constant	96485	C mol^{-1}
z	Valency of Ca^{2+} ions	2	
A_O	Area of Orai channel	0.25 [52]	nm^2
V_{max}	SERCA2b pump rate	36 [41]	Ca^{2+} ions/s
K_F	SERCA2b pump Ca^{2+} affinity (forward rate)	0.27 [41]	μM
H	Hill coefficient for the SERCA2b pump	1.7 [41]	
V_{max}	SERCA2a pump rate	72 [41]	Ca^{2+} ions/s
K_F	SERCA2a pump Ca^{2+} affinity (forward rate)	0.38 [41]	μM
H	Hill coefficient for the SERCA2a pump	2.2 [41]	
K_R	SERCA pump Ca^{2+} affinity (reverse rate)	1700 [53]	μM
Q	Temperature coefficient	2.6 [53]	

Table A.1: Table of parameter values used in model chosen according to estimates in literature. Distance to PM, ER membrane and bulk ER are defined as the distance from a point of the bulk ER. H and L_2 chosen to ensure height of junction ($H - L_2$) is in agreement with experimental estimates [16]. As discussed in Section 2, the height of the sub-PM ER has not been measured so we have chosen L_0 so that the height of the sub-PM ER is larger than the height of the ER-PM junction.

Parameter	Description	Value	Unit
$\triangle t$	Size of time step	1	μs
$\triangle r$	Radial step size	0.2	nm
$\triangle \phi$	Angular step size for clustered Orai channel configuration	0.0419	radians
$\triangle z_{\mathrm{J}}$	z step size in ER-PM junction	0.15	nm
$\triangle z_{\mathrm{S}}$	z step size in sub-PM ER	4.85	nm
σ_ϕ	Angular standard deviation of Gaussian, $w(r, \phi)$	0.05	
σ_r	Radial standard deviation of Gaussian, $w(r, \phi)$	0.05	
T	Simulated time	1	ms
N_{Orai}	Number of Orai channels	5	
N_{SERCA}	Number of SERCA pumps	10	

Table A.2: Table of parameter values used in simulations.

the relationship between the cytoplasmic Ca^{2+} dynamics and the Ca^{2+} concentrations of the sub-PM ER and bulk ER, highlighting the importance of the Ca^{2+} dynamics of the ER-PM junction on the sub-PM ER Ca^{2+} concentrations and ER refilling. This model used an ordinary differential equation (ODE) framework which averaged the Ca^{2+} concentrations in the compartments. In our model we use a partial differential equation (PDE) framework to simulate the spatial Ca^{2+} profiles generated in the ER-PM junction and sub-PM ER thus allowing investigation into how the spatial localisation of Orai channels and SERCA pumps and local Ca^{2+} dynamics affect ER refilling.

The model presented by Samanta *et al.* [25] describes spatial Ca^{2+} profiles in the ER-PM junction. On the surface this model is similar to ours, however, the models are formulated in different manners. Samanta *et al.*

prescribe no flux boundary conditions on all the the boundaries of the domain and include an internal source term to describe Ca^{2+} influx through Orai channels. Whereas we approximate the Ca^{2+} flux through each Orai channel or SERCA pump as a boundary flux through a single grid element, as shown in Figure 2(b), on the PM and ER membrane, respectively. We also prescribe a Dirichlet boundary condition at the edge of the ER-PM junction to ensure the Ca^{2+} concentration within the junction is continuous with the concentration of the bulk cytoplasm. We compare the effect of SERCA2a and SERCA2b pumps on ER refilling using the kinetic parameters given by Lytton *et al.* [41].

We define the geometry of the ER-PM junction and sub-PM ER in Section 2 as cylinders of radius a and assume the PM is at $z = H$, the ER membrane at $z = L_2$ and the interface between the sub-PM ER and bulk ER at $z = L_1$. The Ca^{2+} influx through the Orai channels, F_{Orai}, is calculated using the magnitude of the single Orai current, 2.1fA, observed experimentally by Hoth and Penner [1] using patch clamp techniques and further confirmed using a noise analysis approach by Zweifach and Lewis [39]. We use Faraday's law of electrolysis and calculate the flux per unit area per Orai channel,

$$F_{\text{Orai}} = \frac{I_{\text{Orai}}}{FzA_{\text{O}}},$$

where I_{Orai} is the magnitude of the Orai current per channel, F is Faraday's constant, z is the valency of Ca^{2+} and A_{O} is the area of the Orai channel. Ca^{2+} influx through an Orai channel is approximated to Ca^{2+} influx through a grid element, seen in Figure 2(b) and discussed in Section 2. This grid element has approximately the same area as an Orai channel, 0.25nm^2 [52],

to ensure the total flux per Orai channel is conserved. When we investigate the non-clustered Orai channels we must implement a smaller ϕ mesh ($\triangle\phi = 0.0251$, $\sigma_\phi = 0.03$) to ensure the area of the grid element is still approximately the same size as the area of the Orai channel. If we do not refine the mesh we will not conserve the total flux and the grid element approximating the non-clustered Orai channel will have a larger area than the Orai channel pore and thus result in larger Ca^{2+} influx through the non-clustered grid elements. This is a consequence of the non-uniform spatial discretisation of the cylinder.

The SERCA pumps transport Ca^{2+} from the ER-PM junction into the sub-PM ER. The SERCA pump transport system depends on the Ca^{2+} concentrations on either side of the membrane so we use a bidirectional SERCA pump model [53] to account for the Ca^{2+} concentrations on both sides of the membrane using the binding coefficients given by Lytton [41]. The Ca^{2+} flux per unit area per SERCA pump is given by,

$$F_{\text{SERCA}} = \frac{Q}{A_{\text{S}}} \frac{V_{\max} \left(C_J/K_F\right)^H - V_{\max} \left(C_S/K_R\right)^H}{1 + \left(C_J/K_F\right)^H + \left(C_S/K_R\right)^H},$$

where $V_{\max}$ is the maximal pump rate, Q is the temperature coefficient, A_{S} is the area of the grid element the SERCA flux enters through, H is the Hill coefficient, K_F and K_R are the forward and reverse binding coefficients and C_J and C_S are the Ca^{2+} concentrations of the ER-PM junction and sub-PM ER, respectively.

Ca^{2+} diffusion in the ER-PM junction, $C_{\text{J}} = C_{\text{J}}\left(r, \phi, z, t\right)$, is governed by

the diffusion equation,

$$\frac{\partial C_{\mathrm{J}}}{\partial t} = D_{\mathrm{J}} \nabla^2 C_{\mathrm{J}}, \tag{A.1}$$

with the following initial ($C_{\mathrm{J},0}$) and boundary conditions,

$$\begin{aligned} C_{\mathrm{J},0} = 0.1\mu\mathrm{M}, \qquad & D_{\mathrm{J}} \frac{\partial C_{\mathrm{J}}}{\partial z}\bigg|_{z=H} = F_{\mathrm{Orai}} w(r_{\mathrm{Orai}}, \phi_{\mathrm{Orai}}), \\ C_{\mathrm{J}}\bigg|_{r=a} = 0.1\mu\mathrm{M}, \qquad & D_{\mathrm{J}} \frac{\partial C_{\mathrm{J}}}{\partial z}\bigg|_{z=L_2} = F_{\mathrm{SERCA}} w(r_{\mathrm{SERCA}}, \phi_{\mathrm{SERCA}}), \end{aligned} \tag{A.2}$$

where $(r_{\mathrm{Orai}}, \phi_{\mathrm{Orai}})$ and $(r_{\mathrm{SERCA}}, \phi_{\mathrm{SERCA}})$ positions the Orai channel and SERCA pump, respectively, on the grid. We include five Orai channels and ten SERCA pumps in our simulations, as discussed in Section 2. We include Ca^{2+} fluxes into the model via,

$$w(r_i, \phi_i) = \exp\left(-\left((r - r_i)/\sigma_r\right)^2 - \left((\phi - \phi_i)/\sigma_\phi\right)^2\right),$$

which corresponds to a spatially extended Ca^{2+} channel or SERCA pump centred at (r_i, ϕ_i) for $i \in \{\mathrm{Orai}, \mathrm{SERCA}\}$. Here σ_r and σ_ϕ control the width in the r and angular directions, respectively.

Ca^{2+} diffusion in the sub-PM ER, $C_{\mathrm{S}} = C_{\mathrm{S}}(r, \phi, z, t)$, is governed by the diffusion equation,

$$\frac{\partial C_{\mathrm{S}}}{\partial t} = D_{\mathrm{ER}} \nabla^2 C_{\mathrm{S}}, \tag{A.3}$$

with the following initial ($C_{\mathrm{S},0}$) and boundary conditions:

$$\begin{aligned} C_{\mathrm{S},0} = 150\mu\mathrm{M}, \qquad & D_{\mathrm{ER}} \frac{\partial C_{\mathrm{S}}}{\partial z}\bigg|_{z=L_2} = F_{\mathrm{SERCA}} w(r_{\mathrm{SERCA}}, \phi_{\mathrm{SERCA}}), \\ C_{\mathrm{S}}\bigg|_{z=L_1} = 150\mu\mathrm{M}, \qquad & D_{\mathrm{ER}} \frac{\partial C_{\mathrm{S}}}{\partial r}\bigg|_{r=a} = 0. \end{aligned} \tag{A.4}$$

We solve the PDE systems according to the methods in [54, 55]. In the following, the Ca^{2+} concentration, C_x, where $x \in \{\mathrm{J}, \mathrm{S}\}$ denotes the Ca^{2+} concentration of the ER-PM junction (J) or the sub-PM ER (S). To evaluate the temporal evolution of the Ca^{2+} concentration we discretise time using a time step, $\triangle t$, and write $t = (t_0, t_1, ..., t_n = T)$. We can then describe the Ca^{2+} concentration at time t_i using the Ca^{2+} concentration of the previous time step, t_{i-1},

$$C_{x,t_i} = \int_V G_x \left(C_{x,t_{i-1}} - W_x \right) \mathrm{d}V' + W_x, \tag{A.5}$$

where $G_x = G_x(r, r', \phi, \phi', z, z', \triangle t)$ represents the Green's function of the domain, V is the volume of the domain and $W_x = W_x(r, \phi, z)$ represents the steady state solution of the domain. The Green's function propagates the effect of the initial condition and boundary condition over one time step, $\triangle t$. The solution describes the change in Ca^{2+} concentration over one time step due to the diffusion of the previous Ca^{2+} profile and Ca^{2+} fluxes across the boundaries. We then time step the solution and iterate equation (A.5) to find the Ca^{2+} concentration at each time step thus approximating the temporal evolution of the Ca^{2+} concentration.

We pre-compute the Green's function of each domain in MATLAB and pre-compute the integral,

$$W_x - \int_V G_x W_x \mathrm{d}V', \tag{A.6}$$

so that during each time step of the simulation we only integrate over the previous Ca^{2+} concentration, $C_{x,t_{i-1}}$, which propagates the Ca^{2+} concentra-

tion from the previous time step, and add equation (A.6), which propagates the boundary condition over that time step. This reduces the computational intensity per time step of the simulation.

The Green's function in the ER-PM junction is given by,

$$
\begin{aligned}
&G_{\mathrm{J}}\left(r, r', \phi, \phi', z, z', \triangle t\right) = \\
&\frac{1}{\pi a^2 (H - L_2)} \left[1 + 2\sum_{m=1}^{M_{\mathrm{J}}} \cos\left(\mu_m \left(z' - L_2\right)\right) \cos\left(\mu_m \left(z - L_2\right)\right) \exp\left(-D_J \mu_m^2 \triangle t\right)\right] \\
&\times \sum_{k=1}^{K_{\mathrm{J}}} \left[\frac{J_0\left(\alpha_{0,k} r'/a\right) J_0\left(\alpha_{0,k} r/a\right)}{J_1\left(\alpha_{0,k}\right)^2} \exp\left(-D_J \left(\alpha_{0,k}/a\right)^2 \triangle t\right)\right. \\
&\left. + 2\sum_{n=1}^{N_{\mathrm{J}}} \frac{J_n\left(\alpha_{n,k} r'/a\right) J_n\left(\alpha_{n,k} r/a\right)}{J_{n+1}\left(\alpha_{n,k}\right)^2} \cos\left(n\left(\phi - \phi'\right)\right) \exp\left(-D_J \left(\alpha_{n,k}/a\right)^2 \triangle t\right)\right],
\end{aligned}
\tag{A.7}
$$

where $\mu_m = m\pi/(H - L_2)$ for $m = 1, 2, ..., M_{\mathrm{J}}$ and $\alpha_{n,k}$ satisfies $J_n\left(\alpha_{n,k}\right) = 0$ for $k = 1, 2, ..., K_{\mathrm{J}}$, where $J_n(x)$ are Bessel's functions of order n. We use the parameters $M_{\mathrm{J}} = 100$, $K_{\mathrm{J}} = 500$ and $N_{\mathrm{J}} = 75$ in the clustered Orai configuration ($\triangle\phi = 0.0419$) or $N_{\mathrm{J}} = 125$ in the non-clustered Orai configuration ($\triangle\phi = 0.0251$) when calculating the Green's function with $\triangle r$ and $\triangle z_{\mathrm{J}}$ given in Table A.2. The Green's function in the sub-PM ER is given

by,

$$
\begin{aligned}
&G_{\mathrm{S}}\left(r, r', \phi, \phi', z, z', \triangle t\right) = \\
&\frac{2}{\pi a^2 (L_2 - L_1)} \left[\sum_{m=1}^{M_{\mathrm{S}}} \cos\left(\mu_m \left(L_2 - z'\right)\right) \cos\left(\mu_m \left(L_2 - z\right)\right) \exp\left(-D_s \mu_m^2 \triangle t\right) \right] \\
&\times \sum_{k=1}^{K_{\mathrm{S}}} \left[\frac{J_0\left(\beta_{0,k} r'/a\right) J_0\left(\beta_{0,k} r/a\right)}{J_0\left(\beta_{0,k}\right)^2} \exp\left(-D_s \left(\beta_{0,k}/a\right)^2 \triangle t\right) \right. \\
&\left. + \sum_{n=1}^{N_{\mathrm{S}}} \frac{J_n\left(\beta_{n,k} r'/a\right) J_n\left(\beta_{n,k} r/a\right)}{J_n\left(\beta_{n,k}\right)^2 \left(1 - \frac{n^2}{\beta_{n,k}^2}\right)} \cos\left(n\left(\phi - \phi'\right)\right) \exp\left(-D_s \left(\beta_{n,k}/a\right)^2 \triangle t\right) \right],
\end{aligned}
\tag{A.8}
$$

where $\mu_m = (2m-1)\pi/(2(L_2 - L_1))$ for $m = 1, 2, ..., M_{\mathrm{S}}$ and $\beta_{n,k}$ satisfies $J_n'\left(\beta_{n,k}\right) = 0$ for $k = 1, 2, ..., K_{\mathrm{S}}$. We use $M_{\mathrm{S}} = 100$, $K_{\mathrm{S}} = 500$ and $N_{\mathrm{S}} = 75$ in the clustered Orai configuration ($\triangle\phi = 0.0419$) or $N_{\mathrm{S}} = 125$ in the non-clustered Orai configuration ($\triangle\phi = 0.0251$) when calculating the Green's function with with $\triangle r$ and $\triangle z_{\mathrm{S}}$ given in Table A.2.

We implement this method in MATLAB and use matrix multiplications, to compute integrals, and matrix additions to include equation (A.6), which are not computationally expensive. One key limitation of this approach is that the size of the spatial discretisation needed for the Orai channels in the non-clustered configuration increases the length of time the simulations take. We have used a finer mesh to ensure the spatial resolution around the channels is the same in both the clustered and non-clustered Orai configurations. However, this increases the computational intensity and memory requirements of the non-clustered Orai channel solution. The simulations were ran on one CPU core of a Dell R630 server with 2 x

Intel(R) Xeon(R) E5-2660 v4 processors and 768Gb RAM. The clustered Orai channel simulations involved a load time (to load the precomputed variables into MATLAB) of 10 hours with a run time (the time to run the simulations) of 20 hours and used approximately 30% of the available RAM. However, the finer spatial discretisation used when the Orai channel were not clustered led to a load time of 50 hours and a run time of 60 hours and used approximately 60% of the available RAM. The code is available on GitHub at `https://github.com/emmamcivor/supplementary/tree/master/mcivor_three_2018` and instructions for running the code are provided.

References

[1] M. Hoth, R. Penner, Depletion of intracellular calcium stores activates a calcium current in mast cells, Nature 355 (1992) 353–356.

[2] J. W. Putney, N. Steinckwich-Besançon, T. Numaga-Tomita, F. M. Davis, P. N. Desai, D. M. D'Agostin, S. Wu, G. S. Bird, The functions of store-operated calcium channels, Biochim. Biophys. Acta, Mol. Cell. Res. (2016).

[3] J. Soboloff, B. S. Rothberg, M. Madesh, D. L. Gill, STIM proteins: dynamic calcium signal transducers, Nat. Rev. Mol. Cell Biol. 13 (2012) 549–565.

[4] R. S. Lewis, Store-operated calcium channels: new perspectives on mechanism and function, Cold Spring Harbor Perspectives in Biology 3 (2011) a003970.

[5] P. G. Hogan, R. S. Lewis, A. Rao, Molecular basis of calcium signaling in lymphocytes: STIM and ORAI, Annu. Rev. Immunol. 28 (2009) 491–533.

[6] J. W. Putney, The physiological function of store-operated calcium entry, Neurochem. Res. 36 (2011) 1157–1165.

[7] I. F. Abdullaev, J. M. Bisaillon, M. Potier, J. C. Gonzalez, R. K. Motiani, M. Trebak, Stim1 and Orai1 mediate CRAC currents and store-operated calcium entry important for endothelial cell proliferation, Circ. Res. 103 (2008) 1289–1299.

[8] J. Stiber, A. Hawkins, Z.-S. Zhang, S. Wang, J. Burch, V. Graham, C. C. Ward, M. Seth, E. Finch, N. Malouf, et al., STIM1 signalling controls store-operated calcium entry required for development and contractile function in skeletal muscle, Nat. Cell Biol. 10 (2008) 688–697.

[9] C. Gómez-Fernández, A. M. López-Guerrero, E. Pozo-Guisado, I. S. Álvarez, F. J. Martín-Romero, Calcium signaling in mouse oocyte maturation: the roles of STIM1, ORAI1 and SOCE, Mol. Hum. Reprod. 18 (2011) 194–203.

[10] S. Feske, Y. Gwack, M. Prakriya, S. Srikanth, S.-H. Puppel, B. Tanasa, P. G. Hogan, R. S. Lewis, M. Daly, A. Rao, A mutation in Orai1 causes immune deficiency by abrogating CRAC channel function, Nature 441 (2006) 179–185.

[11] J. Hartmann, R. M. Karl, R. P. Alexander, H. Adelsberger, M. S. Brill, C. Rühlmann, A. Ansel, K. Sakimura, Y. Baba, T. Kurosaki, et al.,

STIM1 controls neuronal Ca^{2+} signaling, mGluR1-dependent synaptic transmission, and cerebellar motor behavior, Neuron 82 (2014) 635–644.

[12] M. D. Cahalan, S. L. Zhang, A. V. Yeromin, K. Ohlsen, J. Roos, K. A. Stauderman, Molecular basis of the CRAC channel, Cell Calcium 42 (2007) 133–144.

[13] S. L. Zhang, A. V. Yeromin, X. H.-F. Zhang, Y. Yu, O. Safrina, A. Penna, J. Roos, K. A. Stauderman, M. D. Cahalan, Genome-wide RNAi screen of Ca^{2+} influx identifies genes that regulate Ca^{2+} release-activated Ca^{2+} channel activity, Proc. Nat. Acad. Sci. 103 (2006) 9357–9362.

[14] M. M. Wu, E. D. Covington, R. S. Lewis, Single-molecule analysis of diffusion and trapping of STIM1 and Orai1 at endoplasmic reticulum-plasma membrane junctions, Mol. Biol. Cell 25 (2014) 3672–3685.

[15] J. Liou, M. L. Kim, W. Do Heo, J. T. Jones, J. W. Myers, J. E. Ferrell, T. Meyer, STIM is a Ca^{2+} sensor essential for Ca^{2+}-store-depletion-triggered Ca^{2+} influx, Curr. Biol. 15 (2005) 1235–1241.

[16] M. M. Wu, J. Buchanan, R. M. Luik, R. S. Lewis, Ca^{2+} store depletion causes STIM1 to accumulate in ER regions closely associated with the plasma membrane, J. Cell. Biol. 174 (2006) 803–813.

[17] S. L. Zhang, Y. Yu, J. Roos, J. A. Kozak, T. J. Deerinck, M. H. Ellisman, K. A. Stauderman, M. D. Cahalan, STIM1 is a Ca^{2+} sensor that activates CRAC channels and migrates from the Ca^{2+} store to the plasma membrane, Nature 437 (2005) 902–905.

[18] R. M. Luik, M. M. Wu, J. Buchanan, R. S. Lewis, The elementary unit of store-operated Ca^{2+} entry: local activation of CRAC channels by STIM1 at ER-plasma membrane junctions, J. Cell. Biol. 174 (2006) 815–825.

[19] C. Y. Park, P. J. Hoover, F. M. Mullins, P. Bachhawat, E. D. Covington, S. Raunser, T. Walz, K. C. Garcia, R. E. Dolmetsch, R. S. Lewis, STIM1 clusters and activates CRAC channels via direct binding of a cytosolic domain to Orai1, Cell 136 (2009) 876–890.

[20] P. B. Stathopulos, G.-Y. Li, M. J. Plevin, J. B. Ames, M. Ikura, Stored Ca^{2+} Depletion-induced Oligomerization of Stromal Interaction Molecule 1 (STIM1) via the EF-SAM Region. An initiation mechanism for capacitative Ca^{2+} entry, J. Biol. Chem. 281 (2006) 35855–35862.

[21] P. Várnai, B. Tóth, D. J. Tóth, L. Hunyady, T. Balla, Visualization and manipulation of plasma membrane-endoplasmic reticulum contact sites indicates the presence of additional molecular components within the STIM1-Orai1 Complex, J. Biol. Chem. 282 (2007) 29678–29690.

[22] P. G. Hogan, The STIM1–ORAI1 microdomain, Cell calcium 58 (2015) 357–367.

[23] N. Demaurex, D. Guido, The Role of Mitochondria in the Activation/Maintenance of SOCE: Membrane Contact Sites as Signaling Hubs Sustaining Store-Operated Ca^{2+} Entry, in: Store-Operated Ca^{2+} Entry (SOCE) Pathways, Springer, 2017, pp. 277–296.

[24] W. Ji, P. Xu, Z. Li, J. Lu, L. Liu, Y. Zhan, Y. Chen, B. Hille, T. Xu, L. Chen, Functional stoichiometry of the unitary calcium-release-activated calcium channel, Proc. Nat. Acad. Sci. 105 (2008) 13668–13673.

[25] K. Samanta, P. Kar, G. R. Mirams, A. B. Parekh, Ca^{2+} channel relocalization to plasma-membrane microdomains strengthens activation of Ca^{2+}-dependent nuclear gene expression, Cell Rep. 12 (2015) 203–216.

[26] A. B. Parekh, Ca^{2+} microdomains near plasma membrane Ca^{2+} channels: impact on cell function, J. Physiol. 586 (2008) 3043–3054.

[27] I. M. Manjarrés, A. Rodríguez-García, M. T. Alonso, J. García-Sancho, The sarco/endoplasmic reticulum Ca^{2+} ATPase (SERCA) is the third element in capacitative calcium entry, Cell Calcium 47 (2010) 412–418.

[28] I. M. Manjarrés, M. T. Alonso, J. García-Sancho, Calcium entry-calcium refilling (CECR) coupling between store-operated Ca^{2+} entry and sarco/endoplasmic reticulum Ca^{2+}-ATPase, Cell Calcium 49 (2011) 153–161.

[29] M. T. Alonso, I. M. Manjarrés, J. García-Sancho, Privileged coupling between Ca^{2+} entry through plasma membrane store-operated Ca^{2+} channels and the endoplasmic reticulum Ca^{2+} pump, Mol. Cell. Endocrinol. 353 (2012) 37–44.

[30] A. Sampieri, A. Zepeda, A. Asanov, L. Vaca, Visualizing the store-operated channel complex assembly in real time: identification of SERCA2 as a new member, Cell Calcium 45 (2009) 439–446.

[31] H. Dingsdale, E. Okeke, L. Haynes, G. Lur, A. V. Tepikin, New Aspects of the Contribution of ER to SOCE Regulation: The Role of the ER and ER-Plasma Membrane Junctions in the Regulation of SOCE, in: Store-Operated Ca^{2+} Entry (SOCE) Pathways, Springer, 2017, pp. 217–237.

[32] J. Di Capite, S. W. Ng, A. B. Parekh, Decoding of cytoplasmic Ca^{2+} oscillations through the spatial signature drives gene expression, Curr. Biol. 19 (2009) 853–858.

[33] O. H. Petersen, R. Courjaret, K. Machaca, Ca^{2+} tunnelling through the ER lumen as a mechanism for delivering Ca^{2+} entering via store-operated Ca^{2+} channels to specific target sites, J. Physiol. 595 (2017) 2999–3014.

[34] H. L. Ong, X. Liu, K. Tsaneva-Atanasova, B. B. Singh, B. C. Bandyopadhyay, W. D. Swaim, J. T. Russell, R. S. Hegde, A. Sherman, I. S. Ambudkar, Relocalization of STIM1 for activation of store-operated Ca^{2+} entry is determined by the depletion of subplasma membrane endoplasmic reticulum Ca^{2+} store, J. Biol. Chem. 282 (2007) 12176–12185.

[35] H. Croisier, X. Tan, J. F. Perez-Zoghbi, M. J. Sanderson, J. Sneyd, B. S. Brook, Activation of store-operated calcium entry in airway smooth muscle cells: insight from a mathematical model, PLoS One 8 (2013) e69598.

[36] J. Sneyd, K. Tsaneva-Atanasova, D. Yule, J. Thompson, T. Shuttleworth, Control of calcium oscillations by membrane fluxes, Proc. Nat. Acad. Sci. U.S.A. 101 (2004) 1392–1396.

[37] J. Liou, M. Fivaz, T. Inoue, T. Meyer, Live-cell imaging reveals sequential oligomerization and local plasma membrane targeting of stromal interaction molecule 1 after Ca^{2+} store depletion, Proc. Nat. Acad. Sci. 104 (2007) 9301–9306.

[38] J. L. Dynes, A. Amcheslavsky, M. D. Cahalan, Genetically targeted single-channel optical recording reveals multiple Orai1 gating states and oscillations in calcium influx, Proc. Nat. Acad. Sci. 113 (2016) 440–445.

[39] A. Zweifach, R. S. Lewis, Mitogen-regulated Ca^{2+} current of T lymphocytes is activated by depletion of intracellular Ca^{2+} stores, Proc. Nat. Acad. Sci. 90 (1993) 6295–6299.

[40] A. F. Fomina, C. M. Fanger, J. A. Kozak, M. D. Cahalan, Single channel properties and regulated expression of Ca^{2+} release-activated Ca^{2+} (CRAC) channels in human T cells, J. Cell Biol. 150 (2000) 1435–1444.

[41] J. Lytton, M. Westlin, S. E. Burk, G. E. Shull, D. H. MacLennan, Functional comparisons between isoforms of the sarcoplasmic or endoplasmic reticulum family of calcium pumps, J. Biol. Chem 267 (1992) 14483–14489.

[42] N. L. Allbritton, T. Meyer, L. Stryer, Range of messenger action of calcium ion and inositol 1, 4, 5-trisphosphate, Science 258 (1992) 1812–1812.

[43] S. Means, A. J. Smith, J. Shepherd, J. Shadid, J. Fowler, R. J. Wojcikiewicz, T. Mazel, G. D. Smith, B. S. Wilson, Reaction diffusion

modeling of calcium dynamics with realistic ER geometry, Biophys. J 91 (2006) 537–557.

[44] M. J. Dayel, E. F. Hom, A. Verkman, Diffusion of green fluorescent protein in the aqueous-phase lumen of endoplasmic reticulum, Biophys. J 76 (1999) 2843–2851.

[45] P. Swietach, K. W. Spitzer, R. D. Vaughan-Jones, Ca^{2+}-mobility in the sarcoplasmic reticulum of ventricular myocytes is low, Biophys. J. 95 (2008) 1412–1427.

[46] E. Neher, Usefulness and limitations of linear approximations to the understanding of Ca^{2+} signals, Cell Calcium 24 (1998) 345–357.

[47] R. M. Luik, B. Wang, M. Prakriya, M. M. Wu, R. S. Lewis, Oligomerization of STIM1 couples ER calcium depletion to CRAC channel activation, Nature 454 (2008) 538.

[48] S. Srikanth, Y. Gwack, Orai1-NFAT signalling pathway triggered by T cell receptor stimulation, Mol. Cells 35 (2013) 182–194.

[49] H. Jousset, M. Frieden, N. Demaurex, STIM1 knockdown reveals that store-operated Ca^{2+} channels located close to sarco/endoplasmic Ca^{2+} ATPases (SERCA) pumps silently refill the endoplasmic reticulum, J. Biol. Chem. 282 (2007) 11456–11464.

[50] L. Dode, J. P. Andersen, N. Leslie, J. Dhitavat, B. Vilsen, A. Hovnanian, Dissection of the functional differences between sarco (endo)

plasmic reticulum Ca^{2+}-ATPase (SERCA) 1 and 2 isoforms and characterization of Darier disease (SERCA2) mutants by steady-state and transient kinetic analyses, J. Biol. Chem. 278 (2003) 47877–47889.

[51] Y. Zhou, X. Cai, R. M. Nwokonko, N. A. Loktionova, Y. Wang, D. L. Gill, The STIM-Orai coupling interface and gating of the Orai1 channel, Cell Calcium (2017).

[52] A. B. Parekh, J. W. Putney Jr, Store-operated calcium channels, Physiol. Rev 85 (2005) 757–810.

[53] T. R. Shannon, F. Wang, J. Puglisi, C. Weber, D. M. Bers, A mathematical treatment of integrated Ca^{2+} dynamics within the ventricular myocyte, Biophys. J. 87 (2004) 3351–3371.

[54] G. N. Felder, K. M. Felder, Mathematical methods in engineering and physics, John Wiley & Sons, 2015.

[55] H. Carslaw, J. Jaeger, Heat in Solids, volume 1, Clarendon Press, Oxford, 1959.